Title

An efficient metamodeling approach for uncertainty quantification of complex systems with arbitrary parameter probability distributions

Journal

International Journal for Numerical Methods in Engineering, 109(5)

ISSN

0029-5981

Authors

Wan, Hua-Ping
Ren, Wei-Xin
Todd, Michael D

Publication Date

2017-02-03

DOI

10.1002/nme.5305

Peer reviewed

INTERNATIONAL JOURNAL FOR NUMERICAL METHODS IN ENGINEERING
Int. J. Numer. Meth. Engng 0000; **00**:1–22
Published online in Wiley InterScience (www.interscience.wiley.com). DOI: 10.1002/nme

An efficient metamodeling approach for uncertainty quantification of complex systems with arbitrary parameter probability distributions

Hua-Ping Wan[1], Wei-Xin Ren[1*], Michael D. Todd[2]

[1] *School of Civil Engineering, Hefei University of Technology, Hefei, Anhui Province 230009, China*
[2] *Department of Structural Engineering, University of California, San Diego, 9500 Gilman Dr. 0085, La Jolla, CA 92093-0085, USA*

SUMMARY

This paper proposes an efficient metamodeling approach for UQ of complex system based on Gaussian process model (GPM). The proposed GPM-based method is able to efficiently and accurately calculate the mean and variance of model outputs with uncertain parameters specified by arbitrary probability distributions. Due to the use of GPM, the closed form expressions of mean and variance can be derived by decomposing high-dimensional integrals into one-dimensional integrals. This paper details on how to efficiently compute the one-dimensional integrals. When the parameters are either uniformly- or normally distributed, the one-dimensional integrals can be analytically evaluated, while when parameters do not follow normal or uniform distributions, this paper adopts the effective Gaussian quadrature technique for the fast computation of the one-dimensional integrals. As a result, the developed GPM method is able to calculate mean and variance of model outputs in an efficient manner independent of parameter distributions. The proposed GPM method is applied to a collection of examples. And its accuracy and efficiency is compared with Monte Carlo simulation (MCS), which is used as benchmark solution. Results show that the proposed GPM method is feasible and reliable for efficient UQ of complex systems in terms of the computational accuracy and efficiency. Copyright © 0000 John Wiley & Sons, Ltd.

Received ...

KEY WORDS: uncertainty quantification; parameter uncertainty; Gaussian process model; arbitrary probability distribution; Gaussian quadrature

1. INTRODUCTION

Uncertainty is inherent in a variety of complex systems, including spacecraft, automobiles, bridges, wind turbines, and offshore structures, among many others. The sources of uncertainties may be categories into four groups: model uncertainty, numerical uncertainty, measurement uncertainty, and parameter uncertainty. In general, these uncertainties can be either purely *aleatory*, purely *epistemic*, or a mixture of both. Parameter uncertainty, one of the most studied types of uncertainty, is the focus of this study. Parameter uncertainty can arise due to a number of factors, including but not limited to manufacturing tolerances, assembly processes, unavoidable variability in operating conditions (e.g., inherent aging and deterioration, corrosive environment), and a lack of complete information (e.g., unknown exact value, ill-defined boundary conditions). In order to gain more precise characterization and interpretation of quantities of interest (QoIs) of physical system, parameter uncertainty should be taken into account within the associated physical/simulation model, which corresponds to the task of uncertainty quantification (UQ). UQ generally refers to the process

*Correspondence to: renwx@hfut.edu.cn

of characterizing the uncertainty in QoIs of physical model propagated from uncertain parameters. Specifically, UQ is to determine the relevant statistical moments (such as mean and/or variance), probability density function (PDF), or the envelope (bounds) of QoIs.

The significance of UQ has been increasingly recognized among the scientific community. Modelers and researchers relies heavily on the important characteristics of physical system for prediction, product design, model verification and validation, and decision making with respect to operations, maintenance, and risk management. Consider, for example, a pedestrian bridge, where it would be essential to know the operational probability that an as-built natural frequency would correspond to (or be close to) human input frequencies. Otherwise, human-induced vibration will make pedestrians uncomfortable and even give rise to safety issues. As a result, it is dangerous to considerate OoIs, which are supposed to be uncertain, as deterministic for conducting the above-mentioned activities. In recent years, there has been a surge of interest in the field of UQ, which remains an active research branch.

The commonly-used and well-known approach for UQ is parameter-sampled Monte Carlo simulation (MCS), which refers to performing UQ directly on the physical/simulation model. MCS for UQ involves three steps. First, it starts with generating an ensemble of samples drawn randomly from the PDFs of the uncertain parameters. Then, an ensemble of the corresponding model evaluations are obtained by entering each sample into solvers, such as finite element analysis (FEA) and computational fluid dynamics (CFD). Finally, relevant QoI performance statistics (PDFs or order statistics) may be extracted from the collected model evaluations. Although straightforward, MCS is extremely time-consuming and prohibitively computationally expensive due to its slow convergence rate with only $\mathcal{O}(N^{-0.5})$, where N is the number of samples. When applied to UQ of complex systems where a single run of simulation model is very computationally demanding, MCS is likely to be unaffordable and impractical. For example, on the desktop platform of DELL Dimension E520 with Pentium (R) D CPU 2.80 GHz, Wan et al. [1] spend 64863 minutes (about 45 days) to quantify the uncertainty in natural frequencies of an arch bridge with structural parameter uncertainty via MCS. Accordingly, the bottleneck of the high computational cost associated with MCS severely hindered its wider application to complex systems. It should be mentioned that MCS is broadly used as benchmark for verification of other UQ methods owing to its generality, robustness, and easy implementation.

To improve the efficiency of MCS for UQ, various effective strategies are investigated, including advanced sampling method (such as Latin hypercube sampling [2] and quasi-Monte Carlo (QMC) [3]), subspace iteration [4], subset simulation [5], etc. These techniques are used to make MCS more efficient but still require many runs of the full model. As a result, metamodeling (”fast surrogate”) techniques that use simpler, low-dimensional mathematical expressions to replace the high-fidelity simulation model are gaining popularity in the context of UQ. Versatile metamodels ranges in complexity from simple regressions to more sophisticated models, such as polynomial response surface, radial basis function, polynomial chaos expansion (PCE), and Gaussian process model (GPM). Among these metamodels, PCE and GPM have been extensively used to alleviate the computational burden of the expensive UQ task. PCE is a metamodeling technique based on the spectral representation of the uncertainty. Based on whether the deterministic solver must be modified or not, the approaches of PCE can be categorized into two groups: stochastic Galerkin (intrusive method) and stochastic collocation (non-intrusive method). PCE, which is constructed based on a rigorous mathematical theory, maintains several appealing merits in dealing with UQ problems. PCE enables the numerical stochastic solution to be expressed as the expansion of orthogonal polynomials that are functions of the random parameters. PCE exhibits fast convergence when the solution dependence on random parameters is smooth, and the convergence rate can be improved by selecting the optimal type of orthogonal polynomial. Furthermore, PCE, being a parametric metamodel, provides a computationally efficient, low-dimensional, explicit mathematical expression to model the input-output relationship of the physical system. As a result, there has been a large volume of research devoted to the use of PCE for UQ; see Refs. [6–16]. Unfortunately, PCE severely suffers from the computational challenge of the *curse of dimensionality* [17], where the number of model evaluations required to build an accurate metamodel grows

DOI: 10.1002/nme

exponentially with the number of random inputs and the approximation order. It is noted that the developed sparse grid and/or adaptive schemes (see e.g., [18–20]) provide a remedy to alleviate the *curse of dimensionality* to some extent. In such circumstance, GPM seems to be more suitable. GPM owns the following attractive merits: (1) it allows modelers to assess the uncertainty of the prediction; (2) it possesses the data-driven property, which enables itself not to be restricted to a certain functional form and guarantees the high flexibility in modeling the complexity of a physical system.

Multiple research efforts are dedicated to using GPM in place of the simulation model combined with MCS to facilitate the daunting task of UQ (see e.g., [21–24]). Moreover, GPM in connection with Kronecker products [25], and PCE [26, 27] are also explored for UQ in recent years. The authors develop an analytical GPM-based UQ method [1], which is able to efficiently and precisely calculate mean and variance of QoIs of the physical system. The core of this proposed method is that the introduction of GPM enables the high-dimensional integrals related to mean and variance of QoIs to be decomposed into the one-dimensional integrals. Therefore, the analytical calculation of these one-dimensional integrals would lead to an analytical computation of mean and variance. However, these one-dimensional integrals can be analytically evaluated only when the parameters are with normal and/or uniform distributions, so the proposed GPM UQ method in Ref. [1] is only suitable for the cases whose parameters follow normal and/or uniform distributions. This study extends that previous work in order to generalize the GPM UQ method to cases of complex systems with arbitrary parameter probability distributions.

The organization of this paper is as follows. Section 2 presents the theoretical background and formulation of GPM. In Section 3, the closed form expressions of mean and variance are presented, and then analytical solution and Gaussian quadrature solution are detailed for the fast calculation of the decomposed one-dimensional integrals, depending on the type of probability distributions of parameters. Section 4 provides a collection of industrial application examples to verify the feasibility of the GPM UQ method. After that, how the computational accuracy and time of the GPM UQ method are affected by the number of Gaussian quadrature points is investigated. Finally, the conclusions of this work are drawn in Section 5.

2. GAUSSIAN PROCESS MODEL

GPM is a very popular machine learning technique that can be used for both regression and classification purposes [28]. The original idea of application of GPM to deterministic computer simulator (noise-free), which returns the same outputs every time if it is given the same inputs, dates back to the work of [29]. The nonparametric GPM is derived from a Bayesian framework. In particular, model outputs are treated as a random function with the associated probability distribution modeled through a Gaussian process (GP) prior; a GP prior combined with Gaussian likelihood yields a posterior GP over prediction at a new point using the maximum likelihood estimate. Instead of following the specific algebraic structure of the input-output relationship (such as polynomial response surface), GPM is fully specified by its mean function and covariance function. The mean function is set to zero because we lack prior knowledge of the overall trend of the latent function [30], and zero mean function can also facilitate the formulation of GPM but without loss of generality. On the other hand, we adopt the popularly used squared exponential covariance function, which is expressed as:

$$C(\mathbf{x}, \mathbf{x}') = \eta^2 \exp\left[-\frac{1}{2}\sum_{k=1}^{d}\left(\frac{x_k - x'_k}{\ell_k}\right)^2\right] \tag{1}$$

where x_k is the k-th component of $\mathbf{x}$, and d is the dimension of input space. The covariance function parameters $\boldsymbol{\Theta} = \{\ell_1, \ell_2, \ldots, \ell_d, \eta\}$ are usually named hyperparameters, which are positive to ensure a valid covariance function.

Consider a training set with n observations, $\mathcal{D} = (\mathbf{X}, \mathbf{Y})$, where $\mathbf{X} = \left[\mathbf{x}_1^\top, \mathbf{x}_2^\top, \ldots, \mathbf{x}_n^\top\right]^\top$ and $\mathbf{Y} = [y_1, y_2, \ldots, y_n]^\top$. Our primary aim is to predict the target y_* at an unobserved input $\mathbf{x}_*$. Based

DOI: 10.1002/nme

on the postulation of GPM that model outputs follow GP prior, training set outputs have a joint Gaussian distribution written as:

$$p(\mathbf{Y}) \sim \mathcal{GP}\left(\mathbf{0}, C(\mathbf{X}, \mathbf{X})\right) \tag{2}$$

and the combination of y_* and $\mathbf{Y}$, denoted as $\mathbf{Y}_* = \left[\mathbf{Y}^\top, y_*\right]^\top$, also follows a joint Gaussian distribution:

$$p(\mathbf{Y}_*) \sim \mathcal{GP}\left(\mathbf{0}, \begin{bmatrix} C(\mathbf{X}, \mathbf{X}) & C(\mathbf{X}, \mathbf{x}_*) \\ C(\mathbf{x}_*, \mathbf{X}) & C(\mathbf{x}_*, \mathbf{x}_*) \end{bmatrix}\right). \tag{3}$$

The posterior predictive distribution over y_* conditioned on the training set results from the Bayes' theorem:

$$p(y_*) = \frac{p(\mathbf{Y}_*)}{p(\mathbf{Y})}. \tag{4}$$

Substituting Eqs. (2) and (3) into Eq. (4) leads to:

$$p(y_*) \sim \mathcal{GP}(\hat{y}_*, \nu_{y_*}) \tag{5}$$

with the mean and the variance given by:

$$\hat{y}_* = \boldsymbol{\alpha}^\top \mathbf{C}_* \tag{6}$$

$$\nu_{y_*} = \eta^2 - \mathbf{C}_*^\top \mathbf{C}^{-1} \mathbf{C}_* \tag{7}$$

where $\mathbf{C}_* = \left[C\left(\mathbf{x}_*, \mathbf{x}_1\right), C\left(\mathbf{x}_*, \mathbf{x}_2\right), \ldots, C\left(\mathbf{x}_*, \mathbf{x}_n\right)\right]^\top$; $\mathbf{C} = C(\mathbf{X}, \mathbf{X})$; $\boldsymbol{\alpha} = \mathbf{C}^{-1}\mathbf{Y}$.

The hyperparamters $\boldsymbol{\Theta}$ that completely govern the GPM may be inferred through maximizing the marginal likelihood (i.e., minimizing negative log marginal likelihood (NLML)) of the training set $\mathcal{D}$:

$$\hat{\boldsymbol{\Theta}} = \arg\min_{\boldsymbol{\Theta}} \mathcal{L}(\boldsymbol{\Theta}). \tag{8}$$

Both the expressions of NLML $\mathcal{L}(\boldsymbol{\Theta})$ and its partial derivatives with respect to the hyperparameters are analytically tractable [28], which are as follows:

$$\mathcal{L}(\boldsymbol{\Theta}) = -\log p(\mathbf{Y}|\mathbf{X}, \boldsymbol{\Theta}) = \frac{1}{2}\mathbf{Y}^\top \mathbf{C}^{-1}\mathbf{Y} + \frac{1}{2}\log|\mathbf{C}| + \frac{n}{2}\log(2\pi) \tag{9}$$

$$\frac{\partial \mathcal{L}(\boldsymbol{\Theta})}{\partial \boldsymbol{\Theta}_i} = \frac{1}{2}\mathrm{tr}\left(\mathbf{C}^{-1}\frac{\partial \mathbf{C}}{\partial \boldsymbol{\Theta}_i}\right) - \frac{1}{2}\mathbf{Y}^\top \mathbf{C}^{-1}\frac{\partial \mathbf{C}}{\partial \boldsymbol{\Theta}_i}\mathbf{C}^{-1}\mathbf{Y} \tag{10}$$

where $|\bullet|$, $\mathrm{tr}(\bullet)$, and $(\bullet)^\top$ represent the determinant, trace, and transpose operators, respectively.

The conjugate gradient algorithm is used as optimization solver to search the optimal set of hyperparameters $\hat{\boldsymbol{\Theta}}$ corresponding to the minimum of the objective function $\mathcal{L}(\boldsymbol{\Theta})$ defined in Eq. (9). Recall that hyperparameters must be positive to ensure a valid covariance function. To this end, the hyperparameters are log-transformed before estimation and thus unconstrained. Considering that optimization method is likely to get stuck in local minima, the multi-starting point strategy, is adopted for global coverage, combined with the conjugate gradient optimization to quickly find the neighborhood minimum. To be specific, first we randomly generate 100 starting points. Then, the NLML values are computed for the 100 cases and among them 10 starting points corresponding to the smallest NLML values are selected as starting values to run conjugate gradient routine. Finally, the resulting hyperparameters with the smallest NLML values among these 10 pre-selected cases are accepted as the optimal set of hyperparameters $\hat{\boldsymbol{\Theta}}$.

3. EFFICIENT UNCERTAINTY QUANTIFICATION USING GPM

3.1. Methodology

Consider a physical system with multiple uncertain parameters (denoted by the d-dimensional $\mathbf{x}$). And the QoI is the model output of the physical system (denoted by y). The GPM is utilized to model

DOI: 10.1002/nme

the input-output relationship of the physical system. The focus of this paper is the fast computation of mean and variance of QoIs, which are the two important statistical moments commonly used to quantify the variability, within GPM framework. Bear in mind that GP prediction over y is probabilistic, following a Gaussian distribution with mean and variance given in Eqs. (6) and (7), respectively. Therefore, in light of probability theory, the mean and variance can be defined as:

$$\begin{aligned}\mathbb{E}(y) &= \int y\, p(y) dy \\ &= \int y \left[\int p(y|\mathbf{x}, \mathcal{D}) p(\mathbf{x}) d\mathbf{x} \right] dy \\ &= \int \left[\int y\, p(y|\mathbf{x}, \mathcal{D}) dy \right] p(\mathbf{x})\, d\mathbf{x}\end{aligned} \tag{11}$$

$$\begin{aligned}\mathbb{V}(y) &= \int y^2\, p(y) dy - \mathbb{E}^2(y) \\ &= \int y^2 \left[\int p(y|\mathbf{x}, \mathcal{D}) p(\mathbf{x}) d\mathbf{x} \right] dy - \mathbb{E}^2(y) \\ &= \int \left[\int y^2\, p(y|\mathbf{x}, \mathcal{D}) dy \right] p(\mathbf{x}) d\mathbf{x} - \mathbb{E}^2(y).\end{aligned} \tag{12}$$

Since

$$\int y\, p\left(y|\mathbf{x}, \mathcal{D}\right) dy = \hat{y} \tag{13}$$

$$\int y^2\, p\left(y|\mathbf{x}, \mathcal{D}\right) dy = \nu_y + \hat{y}^2, \tag{14}$$

we obtain

$$\mathbb{E}(y) = \int \hat{y}\, p(\mathbf{x})\, d\mathbf{x} \tag{15}$$

$$\mathbb{V}(y) = \int \left(\nu_y + \hat{y}^2\right) p(\mathbf{x})\, d\mathbf{x} - \mathbb{E}^2(y). \tag{16}$$

where $\int \mathcal{F}(\mathbf{x}) p(\mathbf{x}) d\mathbf{x} = \int \cdots \int \mathcal{F}(x_1, \ldots, x_d) p(x_1) \cdots p(x_d) dx_1 \cdots dx_d$ for brevity.

Making use of Eq. (1), we have the rearrangement of Eqs. (6) and (7) as:

$$\hat{y} = c \sum_{i=1}^{n} \alpha_i \prod_{k=1}^{d} \mathcal{N}_{x_k}\left(x_k^i, \ell_k^2\right) \tag{17}$$

$$\nu_y = \eta^2 - c^2 \sum_{j=1}^{n} \sum_{i=1}^{n} \mathbf{C}_{ij}^{-1} \prod_{k=1}^{d} \mathcal{N}_{x_k}\left(x_k^i, \ell_k^2\right) \mathcal{N}_{x_k}\left(x_k^j, \ell_k^2\right) \tag{18}$$

where $c = \eta^2 (2\pi)^{\frac{d}{2}} \prod_{k=1}^{d} \ell_k$; α_i is the i-th element of $\boldsymbol{\alpha}$; $\mathbf{C}_{ij}^{-1}$ denotes the (i,j)-element of $\mathbf{C}^{-1}$; $\mathcal{N}_{x_k}\left(x_k^{i(j)}, \ell_k^2\right) = \frac{1}{\ell_k \sqrt{2\pi}} \exp\left[-\frac{1}{2\ell_k^2} \left(x_k - x_k^{i(j)} \right)^2 \right]$; x_k denotes the k-th parameter of $\mathbf{x}$; $x_k^{i(j)}$ represents the element at the $i(j)$-th row and the k-th column of the sampling matrix $\mathbf{X}$. Note that the subscript * associated with y is removed for notational convenience.

DOI: 10.1002/nme

Substituting Eq. (17) into Eq. (15) gives:

$$\begin{aligned}\mathbb{E}(y) &= \int \left(c \sum_{i=1}^{n} \alpha_i \prod_{k=1}^{d} \mathcal{N}_{x_k} \left(x_k^i, \ell_k^2 \right) \right) p(\mathbf{x})\, d\mathbf{x} \\ &= c \sum_{i=1}^{n} \alpha_i \prod_{k=1}^{d} \int \mathcal{N}_{x_k} \left(x_k^i, \ell_k^2 \right) p(x_k)\, dx_k \\ &= c \sum_{i=1}^{n} \alpha_i \prod_{k=1}^{d} I_k^i.\end{aligned} \tag{19}$$

where x_k denotes the k-th parameter of $\mathbf{x}$; x_k^i represents the element at the i-th row and the k-th column of the sampling matrix $\mathbf{X}$.

And substituting Eqs. (17) and (18) into Eq. (16) results in:

$$\begin{aligned}\mathbb{V}(y) = &\int \left\{ \left[\eta^2 - c^2 \sum_{j=1}^{n} \sum_{i=1}^{n} \mathbf{C}_{ij}^{-1} \prod_{k=1}^{d} \mathcal{N}_{x_k} \left(x_k^i, \ell_k^2 \right) \mathcal{N}_{x_k} \left(x_k^j, \ell_k^2 \right) \right] + \left[\left(c \sum_{i=1}^{n} \alpha_i \prod_{k=1}^{d} \mathcal{N}_{x_k} \left(x_k^i, \ell_k^2 \right) \right)^2 \right] \right\} p(\mathbf{x})\, d\mathbf{x} \\ &- \mathbb{E}^2(y) \\ = &\int \left\{ \left[\left(c \sum_{i=1}^{n} \alpha_i \prod_{k=1}^{d} \mathcal{N}_{x_k} \left(x_k^i, \ell_k^2 \right) \right) \left(c \sum_{j=1}^{n} \alpha_j \prod_{k=1}^{d} \mathcal{N}_{x_k} \left(x_k^j, \ell_k^2 \right) \right) \right] \right. \\ &\left. + \left[\eta^2 - c^2 \sum_{j=1}^{n} \sum_{i=1}^{n} \mathbf{C}_{ij}^{-1} \prod_{k=1}^{d} \mathcal{N}_{x_k} \left(x_k^i, \ell_k^2 \right) \mathcal{N}_{x_k} \left(x_k^j, \ell_k^2 \right) \right] \right\} p(\mathbf{x})\, d\mathbf{x} - \mathbb{E}^2(y) \\ = &\int \left[c^2 \sum_{j=1}^{n} \sum_{i=1}^{n} \alpha_i \alpha_j \prod_{k=1}^{d} \mathcal{N}_{x_k} \left(x_k^i, \ell_k^2 \right) \mathcal{N}_{x_k} \left(x_k^j, \ell_k^2 \right) - c^2 \sum_{j=1}^{n} \sum_{i=1}^{n} \mathbf{C}_{ij}^{-1} \prod_{k=1}^{d} \mathcal{N}_{x_k} \left(x_k^i, \ell_k^2 \right) \mathcal{N}_{x_k} \left(x_k^j, \ell_k^2 \right) \right] \\ &p(\mathbf{x})\, d\mathbf{x} + \eta^2 - \mathbb{E}^2(y) \\ = &\int c^2 \left[\sum_{j=1}^{n} \sum_{i=1}^{n} \left(\alpha_i \alpha_j - \mathbf{C}_{ij}^{-1} \right) \prod_{k=1}^{d} \mathcal{N}_{x_k} \left(x_k^i, \ell_k^2 \right) \mathcal{N}_{x_k} \left(x_k^j, \ell_k^2 \right) \right] p(\mathbf{x})\, d\mathbf{x} + \eta^2 - \mathbb{E}^2(y) \\ = &\int c^2 \left[\sum_{j=1}^{n} \sum_{i=1}^{n} \left(\alpha_i \alpha_j - \mathbf{C}_{ij}^{-1} \right) \prod_{k=1}^{d} \mathcal{N}_{x_k^i} \left(x_k^j, 2\ell_k^2 \right) \mathcal{N}_{x_k} \left(\frac{x_k^i + x_k^j}{2}, \frac{\ell_k^2}{2} \right) \right] p(\mathbf{x})\, d\mathbf{x} + \eta^2 - \mathbb{E}^2(y) \\ = &c^2 \left[\sum_{j=1}^{n} \sum_{i=1}^{n} \left(\alpha_i \alpha_j - \mathbf{C}_{ij}^{-1} \right) \prod_{k=1}^{d} \mathcal{N}_{x_k^i} \left(x_k^j, 2\ell_k^2 \right) \int \mathcal{N}_{x_k} \left(\frac{x_k^i + x_k^j}{2}, \frac{\ell_k^2}{2} \right) p(x_k) dx_k \right] + \eta^2 - \mathbb{E}^2(y) \\ = &c^2 \left[\sum_{j=1}^{n} \sum_{i=1}^{n} \left(\alpha_i \alpha_j - \mathbf{C}_{ij}^{-1} \right) \prod_{k=1}^{d} \mathcal{N}_{x_k^i} \left(x_k^j, 2\ell_k^2 \right) I_k^{ij} \right] + \eta^2 - \mathbb{E}^2(y)\end{aligned} \tag{20}$$

where $x_k^{i(j)}$ represents the element at the $i(j)$-th row and the k-th column of the sampling matrix $\mathbf{X}$.

The derivation of $\mathbb{V}(y)$ makes use of the identity of Gaussian multiplication, that is, the product of two Gaussians gives another (un-normalized) Gaussian [31]:

$$\mathcal{N}_{\mathbf{x}} \left(\boldsymbol{\mu}_1, \boldsymbol{\Sigma}_1 \right) \mathcal{N}_{\mathbf{x}} \left(\boldsymbol{\mu}_2, \boldsymbol{\Sigma}_2 \right) = z \mathcal{N}_{\mathbf{x}} \left(\boldsymbol{\mu}_3, \boldsymbol{\Sigma}_3 \right) \tag{21}$$

where $\boldsymbol{\Sigma}_3 = \left({\boldsymbol{\Sigma}_1}^{-1} + {\boldsymbol{\Sigma}_2}^{-1} \right)^{-1}$; $\boldsymbol{\mu}_3 = \boldsymbol{\Sigma}_3 \left({\boldsymbol{\Sigma}_1}^{-1} \boldsymbol{\mu}_1 + {\boldsymbol{\Sigma}_2}^{-1} \boldsymbol{\mu}_2 \right)$; $z = \mathcal{N}_{\boldsymbol{\mu}_1} \left(\boldsymbol{\mu}_2, \boldsymbol{\Sigma}_1 + \boldsymbol{\Sigma}_2 \right)$.

DOI: 10.1002/nme

As seen in Eqs. (19) and (20), it is known that with the use of GPM, the high-dimensional integrals associated with mean and variance are successfully transformed into the one-dimensional integrals. As long as the one-dimensional integrals can be efficiently calculated, QoI order statistics will be computed very efficiently. As a result, using GPM as a surrogate model of a physical system, the UQ problem will become the task of computing the one-dimensional integrals. Therefore, it is crucial to evaluate these one-dimensional integrals efficiently, while still maintaining high accuracy.

3.2. Efficient calculation of one-dimensional integrals

Integrals of I_k^i and I_k^{ij} can be unified into the following expression:

$$\mathcal{I} = \int \mathcal{N}_x\left(\zeta, \vartheta^2\right)\, p(x)\, dx, \tag{22}$$

3.2.1. Analytical solution When parameter x follows normal or uniform distributions, the above integral may be analytically evaluated [1, 32]; see as follows:

$$\begin{aligned}
\mathcal{I} &= \int \mathcal{N}_x\left(\zeta, \vartheta^2\right)\, p\left(x\right)\, dx \\
&= \begin{cases} \displaystyle\int \mathcal{N}_x\left(\zeta, \vartheta^2\right)\, \mathcal{N}_x\left(\xi, \theta^2\right)\, dx & \text{if } \; x \sim \mathcal{N}\left(\xi, \theta^2\right), \\ \displaystyle\frac{1}{(\overline{x} - \underline{x})} \int \mathcal{N}_x\left(\zeta, \vartheta^2\right)\, dx & \text{if } \; x \sim \mathcal{U}(\overline{x}, \underline{x}). \end{cases} \\
&= \begin{cases} \mathcal{N}_\zeta\left(\xi, \vartheta^2 + \theta^2\right) & \text{if } \; x \sim \mathcal{N}\left(\xi, \theta^2\right), \\ \displaystyle\frac{1}{(\overline{x} - \underline{x})}\left[\Phi\left(\frac{\overline{x} - \zeta}{\vartheta}\right) - \Phi\left(\frac{\underline{x} - \zeta}{\vartheta}\right)\right] & \text{if } \; x \sim \mathcal{U}(\overline{x}, \underline{x}). \end{cases}
\end{aligned} \tag{23}$$

where $\underline{x}$ and $\overline{x}$ are corresponding to lower bound and upper bound of the parameter x, respectively and $\Phi(\bullet)$ denotes the cumulative distribution function of the standard normal distribution.

3.2.2. Gaussian quadrature solution For the cases whose parameters are not normal and uniform distributions, we resort to Gaussian quadrature integration for fast computation of the integral. The implementation procedure regarding computing the integral using Gaussian quadrature is detailed in the following section.

3.2.2.1. Gaussian quadrature formulae Gaussian quadrature is an important numerical integration technique to approximate a definite integral of a given function by a weighted sum of a finite set of function evaluations. An n-point quadrature rule for a given function $f(x)$ and positive measure $w(x)$ is given by:

$$\int f(x)\, w(x)\, dx \approx \sum_{i=1}^{n} w_i f(x_i) \tag{24}$$

where x_i and w_i are called abscissae (nodes) and weights of the Gaussian quadrature rule, respectively. The quadrature on the right side of Eq. (24) gives the exact value of the integral for polynomials of degree less than or equal to $2n-1$. In our case, $w(x)$ and $f(x)$ represent the PDF $p(x)$ of an uncertain parameter and $\mathcal{N}_x\left(\zeta, \vartheta^2\right)$ in Eq. (22), respectively.

3.2.2.2. Calculation of Gaussian quadrature rules Gaussian quadrature rules $\{w_i, x_i\}_{i=1}^n$ only depend on positive measure $w(x)$ and can be obtained from certain orthogonal polynomials. An orthogonal polynomial set is defined by the vanishing of the inner product of any two members of the set with regard to some weight. Defining the inner product on pairs of polynomials f and g with regard to some weight function w as:

$$\langle f, g \rangle = \int f(x)\, g(x)\, w(x)\, dx, \tag{25}$$

DOI: 10.1002/nme

then the orthogonality relations can be expressed as:

$$\langle \psi_m, \psi_n \rangle = \int \psi_m \, \psi_n \, w(x) \, dx = \gamma_n \delta_{mn} \tag{26}$$

where δ_{mn} is a Kronecker delta that is one if $m = n$ and zero otherwise; the normalizing constant γ_n is equal to $\langle \psi_n, \psi_n \rangle$.

Orthogonal polynomial sequence satisfies the well-known three-term recurrence relation [33], which is written in the form:

$$\begin{gathered} \psi_{i+1}(x) = (x - a_i)\psi_i(x) - b_i \psi_{i-1}, \; i = 0, 1, 2, \ldots \\ \psi_{-1}(x) = 0, \; \psi_0(x) = 1 \end{gathered} \tag{27}$$

where

$$a_i = \frac{\langle x \, \psi_i, \psi_i \rangle}{\langle \psi_i, \psi_i \rangle} \qquad i = 0, 1, 2, \ldots \tag{28}$$

$$b_i = \begin{cases} \langle \psi_0, \psi_0 \rangle & i = 0, \\ \dfrac{\langle \psi_i, \psi_i \rangle}{\langle \psi_{i-1}, \psi_{i-1} \rangle} & i = 1, 2, \ldots . \end{cases} \tag{29}$$

are the recurrence coefficients uniquely determined by positive measure $w(x)$.

Gaussian quadrature rules $\{w_i, x_i\}_{i=1}^n$ can be obtained from the eigenvalue decomposition of the symmetric, tridiagonal Jacobi matrix $\mathbf{J}_n$ assembled with the recurrence coefficients $\{a_i, b_i\}$

$$\mathbf{J}_n = \begin{bmatrix} a_0 & \sqrt{b_1} & & & \\ \sqrt{b_1} & a_1 & \sqrt{b_2} & & \\ & \sqrt{b_2} & \ddots & \ddots & \\ & & \ddots & a_{n-2} & \sqrt{b_{n-1}} \\ & & & \sqrt{b_{n-1}} & a_{n-1} \end{bmatrix}. \tag{30}$$

Specifically, if $\mathbf{V}^T \mathbf{J}_n \mathbf{V} = diag(\lambda_1, \lambda_2, \ldots, \lambda_n)$ and $\mathbf{V}^T \mathbf{V} = \mathbf{I}$, in which $\mathbf{I}$ is the $n \times n$ identity matrix, then the desired abscissae $x_i = \lambda_i$ and the weights $w_i = b_0 v_{i,1}^2$, in which $v_{i,1}$ is the first component of the i-th column vector of $\mathbf{V}$.

3.2.2.3. Calculation of the recurrence coefficients From the above description, we know that in order to obtain the Gaussian quadrature rules $\{w_i, x_i\}_{i=1}^n$, the fundamental problem is to compute the recursion coefficients $\{a_i, b_i\}_{i=0}^{n-1}$ associated with orthogonal polynomials. As shown in Tab. I, there exists the exact recurrence coefficients corresponding to some well-known probability distributions [33, 34]. Therefore, for other probability distributions not in Tab. I, efforts have to be made to find the effective technique for calculating the associated recurrence coefficients.

Discretization method is widely considered as a general-purpose and unconditionally stable scheme to determine the recurrence coefficients for arbitrary positive measure [33–35]. The basic idea behind the discretization method is that the given continuous measure can be approximated by a discrete n-point measure if the discretizations are done in a meaningful manner. This discrete measure is given by:

$$\omega_n(x) = \sum_{i=1}^{n} \omega_i \, \delta \left(x - \xi_i \right), \tag{31}$$

which has its weights and abscissae assembled into a sparse matrix

$$\mathbf{A} = \begin{bmatrix} 1 & \sqrt{\omega_1} & \sqrt{\omega_2} & \cdots & \sqrt{\omega_n} \\ \sqrt{\omega_1} & \xi_1 & & & \\ \sqrt{\omega_2} & & \xi_1 & & \\ \vdots & & & \ddots & \\ \sqrt{\omega_n} & & & & \xi_n \end{bmatrix} \tag{32}$$

DOI: 10.1002/nme

that is orthogonally similar to the matrix

$$\mathbf{J} = \begin{bmatrix} 1 & \sqrt{b_0}\,\mathbf{e}_1^\top \\ \sqrt{b_0}\,\mathbf{e}_1 & \mathbf{J}_n \end{bmatrix} \tag{33}$$

where $\mathbf{e}_1^\top = [1, 0, \ldots, 0]_{1\times n}$ and $\mathbf{J}_n$ is the Jacobi matrix expressed in Eq. (30). Considering that the conventional Lanczos algorithm is numerically unstable, Givens rotation technique developed by Gragg and Harrod [36] is adopted for the orthogonal similarity transformation to obtain the recurrence coefficients in the Jacobi matrix $\mathbf{J}_n$. The corresponding implementation details are summarized in their pseudocode RKWW algorithm.

To get the recurrence coefficients, we have to obtain the weights ω_i and abscissae ξ_i with respect to the discrete measure $\omega_n(x)$. In accordance with Eq. (31), the first step is to choose a sequence of measures that converge to the measure $w(x)dx$. Herein, the fast Fejér Type-2 integration scheme, whose weights can be calculated considerably efficiently through the inverse fast Fourier transform [37], is utilized to perform the integral $\int w(x)dx$. Fejér Type-2 rules are very similar to the well-known Clenshaw-Curtis rules over the interval $[-1, 1]$, but Fejér Type-2 rules are open-ended, that is omitting the abscissae -1 and 1, and thus are more suitable for measures with non-compact support. To use the fast Fejér Type-2 integration for $w(x)$ with an arbitrary domain $[l, u]$ (l and u can be either finite or infinite.), a suitable transformation of variables can be used to scale $[l, u]$ into the interval $[-1, 1]$:

$$\int_l^u w(x)\,dx = \int_{-1}^{1} w\left(\phi(\tau)\right)\,\phi'(\tau)\,d\tau. \tag{34}$$

Here we adopt transformation $x = \phi(\tau)$ of Ref. [33] expressed as:

$$\phi(\tau) = \begin{cases} \dfrac{1}{2}(u-l)\tau + \dfrac{1}{2}(u+l) & \text{if} \quad -\infty < l < u < \infty, \\ u - \dfrac{1-\tau}{1+\tau} & \text{if} \quad -\infty = l < u < \infty, \\ l + \dfrac{1+\tau}{1-\tau} & \text{if} \quad -\infty < l < u = \infty, \\ \dfrac{\tau}{1-\tau^2} & \text{if} \quad -\infty = l < u = \infty. \end{cases} \tag{35}$$

Finally, we obtain the abscissae and weights $\{\xi_i = \phi(z_i), \omega_i = q_i\,\omega(z_i)\,\phi'(z_i)\}_{i=1}^n$ for Eq. (31), in which $\{z_i, q_i\}_{i=1}^n$ are corresponding to the abscissae and weights of the Fejér Type-2. Then by performing the orthogonal similarity transformation using Givens rotation technique, the recurrence coefficients $\{a_i, b_i\}_{i=0}^{n-1}$ can be attained. For the sake of guaranteeing the high accuracy in the recurrence coefficients, an iterative process is applied using the following stopping criterion [38]:

$$|b_i^s - b_i^{s-1}| \le \varepsilon\, b_i^s, \quad i = 1, 2, \ldots, n \tag{36}$$

where s is the iteration step and ε is the given error tolerance.

In summary, first, find a discrete measure $\omega_m(x)$ to approximate the continuous measure $w(x)$. Next, Fejér Type-2 integration is utilized to infer the abscissae and weights $\{\xi_i, \omega_i\}_{i=1}^n$ associated with the discrete measure $\omega_m(x)$. Then, Lanczos process using Givens rotation technique is launched to transform $\mathbf{A}$ into $\mathbf{J}$. Finally, we obtain the recurrence coefficients $\{a_i, b_i\}_{i=0}^{n-1}$, which are assembled into $\mathbf{J}_n$. Note that the procedure of calculating the recurrence coefficients will be repeated until the stopping criterion is achieved. The detailed implementation of the recurrence coefficients

DOI: 10.1002/nme

estimation is presented in Algorithm 1.

Algorithm 1: Computation of the recurrence coefficients

Input: No. of the recurrence coefficients n, the positive measure $w(x)$ and the associated support interval $[l, u]$, and the error tolerance ε.

Output: Recurrence coefficients $\{a_i, b_i\}_{i=0}^{n-1}$.

repeat

1: Update $N_s = \begin{cases} 1 + \lfloor (2n-1)/2 \rfloor & \text{if } \ s = 0, \\ N_0 + 1 & \text{if } \ s = 1, \\ N_{s-1} + 2^{\lfloor s/5 \rfloor} n & \text{if } \ s = 2, 3, \ldots. \end{cases}$

2: Evaluate the abscissae and weights $\{z_i, q_i\}_{i=1}^{N_s}$ of the Fejér Type-2.

3: Compute $\{\varepsilon_i, \omega_i\}_{i=1}^{N_s}$ through $\xi_i = \phi(z_i), \omega_i = q_i\, \omega(z_i)\, \phi'(z_i)$.

4: Perform orthogonal similarity transformation ($\mathbf{A} \rightarrow \mathbf{J}$) to obtain the recurrence coefficients $\{a_i, b_i\}_{i=0}^{n-1}$.

until $|b_i^s - b_i^{s-1}| \leq \varepsilon\, b_i^s$;

N_s is determined based on the Ref. [33]; $\lfloor \bullet \rfloor$ returns the nearest integer less than or equal to $\bullet$.

3.2.3. Implementation summary The highlight of the present method for efficient UQ is the use of GPM, which enables us to decompose the high-dimensional integrals related to mean and variance into one-dimensional integrals. Once the one-dimensional integrals can be efficiently computed, the goal of achieving fast and accurate calculation of the mean and variance of QoIs may be attained. Therefore, the efficient and accurate evaluation of the one-dimensional integrals is of great importance. For the case that $p(x)$ is either uniform or normal distribution, the one-dimensional integrals can be evaluated in an analytical way, while for the case that $p(x)$ are not (or cannot be modeled with) normal or uniform distributions, the one-dimensional integrals can be efficiently computed as well via Gaussian quadrature solution. The computation of the one-dimensional integral defined $\mathcal{I}$ in Eq. (22) is detailed in Fig. 1.

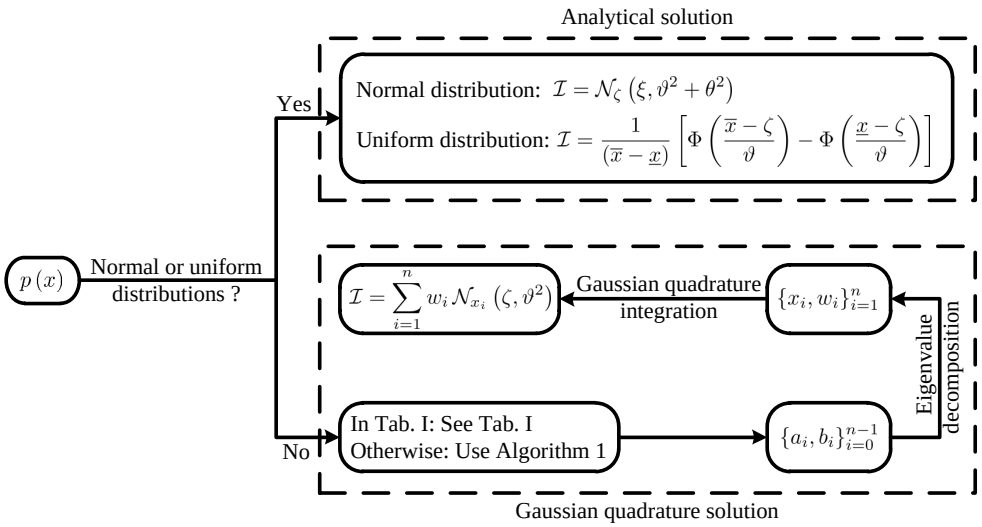

Fig. 1. Flowchart of the computation of the one-dimensional integral $\mathcal{I}$.

DOI: 10.1002/nme

Tab. I. Exact recurrence coefficients for several probability distributions $p(x)$.

Distribution	PDF	Domain	$a_i, i \geq 0$	$b_i, i \geq 1$
Uniform	$\frac{1}{2}$	$[-1, 1]$	0	$\frac{i^2}{4i^2-1}$
Normal	$\frac{1}{\sigma\sqrt{2\pi}} e^{-\frac{(x-\mu)^2}{2\sigma^2}}$	$[-\infty, \infty]$ $\sigma^2 > 0$	μ	$i\,\sigma^2$
Log-normal	$\frac{1}{x\sigma\sqrt{2\pi}} e^{-\frac{(\ln x-\mu)^2}{2\sigma^2}}$	$(0, \infty]$ $\sigma^2 > 0$	$[e^{i\sigma^2}(e^{\sigma^2}+1)-1]e^{\mu+\frac{1}{2}\sigma^2(2i-1)}$	$(e^{i\sigma^2}-1)e^{2\mu+\sigma^2(3i-2)}$
Gamma	$\frac{1}{\Gamma(\alpha)\beta^\alpha} x^{\alpha-1} e^{-\frac{x}{\beta}}$	$(0, \infty]$ $\alpha > 0, \beta > 0$	$\beta(\alpha+2i)$	$i\beta^2(\alpha+i-1)$
Inverse-gamma	$\frac{\beta^\alpha}{\Gamma(\alpha)} x^{-\alpha-1} e^{-\frac{\beta}{x}}$	$(0, \infty]$ $\alpha > 0, \beta > 0$	$\frac{\beta(\alpha+1)}{(\alpha-2i+1)(\alpha-2i-1)}$	$\frac{i\beta^2(\alpha-i+1)}{(\alpha-2i)(\alpha-2i+2)(\alpha-2i+1)^2}$
Beta	$\frac{1}{\mathrm{B}(\alpha,\beta)} x^{\alpha-1}(1-x)^{\beta-1}$	$(0, 1)$ $\alpha > 0, \beta > 0$	$\frac{\alpha(\alpha+\beta)+\alpha(2i-2)+2i\beta+i(2i-2)}{(\alpha+\beta+2i)(\alpha+\beta+2i-2)}$	$\frac{i(\alpha+\beta+i-2)(\alpha+i-1)(\beta+i-1)}{(\alpha+\beta+2i-1)(\alpha+\beta+2i-3)(\alpha+\beta+2i-2)^2}$
Student's t	$\frac{\Gamma(\frac{\nu+1}{2})}{\sqrt{\nu\pi}\Gamma(\frac{\nu}{2})} \left(1+\frac{x^2}{\nu}\right)^{-\frac{\nu+1}{2}}$	$[-\infty, \infty]$ $\nu > 0$	0	$\frac{i\nu(\nu-i+1)}{(\nu-2i)(\nu-2i+2)}$
Fisher's F	$\frac{\sqrt{\frac{(\nu_1 x)^{\nu_1}\,\nu_2^{\nu_2}}{(\nu_1 x+\nu_2)^{\nu_1+\nu_2}}}}{x\mathrm{B}(\frac{\nu_1}{2}, \frac{\nu_2}{2})}$	$[0, \infty]$ $\nu_1 > 0, \nu_2 > 0$	$\frac{\nu_2(\nu_1\nu_2+2\nu_1+4i\nu_2-8i^2)}{\nu_1(\nu_2-4i-2)(\nu_2-4i+2)}$	$\frac{2i\nu_2^2(\nu_1+2i-2)(\nu_2-2i+2)(\nu_1+\nu_2-2i)}{\nu_1^2(\nu_2-4i)(\nu_2-4i+4)(\nu_2-4i+2)^2}$

Note: $b_0 = \langle\psi_0, \psi_0\rangle = \int p(x)\,dx = 1$; By setting $\alpha = 1$, gamma distribution can be transformed into exponential distribution.

3.3. Scope

The proposed approach is based on the use of GPM with zero mean function and squared exponential covariance function. The separable feature of the adopted mean and covariance functions is the key of the approach, since it finally results in the decomposition of the high-dimensional integrals associated with mean and variance into one-dimensional integrals. As for GPM, there are available various mean and covariance functions [28]. Apart from zero mean function, other types of mean functions, such as constant, linear, and polynomial, are available. Obviously, these mentioned mean functions are separable. In contrast with mean function, there exists more versatile covariance functions, including squared exponential, Matérn, exponential, power exponential, periodic, etc. Most of covariance functions are separable, since they can be expressed in the separable form of a product of a sequence of one-dimensional functions. Considering the fact that most of mean and covariance functions are separable, this approach is not restricted to the use of the special GPM, which is defined by zero mean function and squared exponential covariance function.

Bear in mind that within GPM framework, the multi-dimensional integral decomposition can take effect only when the selected mean and covariance functions are both separable. In the situation that either mean function or covariance function (e.g., non-stationary neural network one) is non-separable, MCS and cubature can be used to obtain the mean and variance of QoIs. The GPM-based MCS in conjunction with the advanced sampling strategies (such as Latin hypercube sampling and quasi-Monte Carlo) is a promising alternative for mean and variance calculations. It should be pointed out that the GPM-based MCS allows for evaluating PDF beyond order statistics. For more details on the GPM-based MCS, interested readers are referred to Refs. [21, 23]. Specifically, the cubature is that the d-dimensional integration is treated as a succession of d one-dimensional integrals and apply the one-dimensional quadrature formula d times. This is the idea underlying tensor product quadrature formulae.

4. APPLICATION

This section presents three industrial examples: one composite beam, one auto frame, and one concrete-filled steel tubular (CFST) through arch bridge. The present method is put forward to conduct UQ of the displacement of the composite beam, and the natural frequencies of the auto frame and the CFST through arch bridge. In the meanwhile, MCS is used to assess the computational accuracy and efficiency of the proposed GPM UQ method.

DOI: 10.1002/nme

4.1. Case I: A composite beam

This example of the composite beam, shown in Fig. 2, comes from Ref. [39]. The material of this composite beam is a combination of a fraction f of fibers and a fraction $1-f$ of matrix. The elastic moduli and density of the fiber and matrix materials are denoted by E_f , ρ_f and E_m, ρ_m, respectively. The beam is L long, with a rectangular section $b \times h$. Of interest is the maximal mid-span displacement d, which resulting from the uniformly distributed load q along its length, is determined by the following expression:

$$d = \frac{5}{384}\frac{qL^4}{E_{\text{hom}}I} \tag{37}$$

where the uniformly distributed load q is:

$$q = \rho_{\text{hom}} gbh; \tag{38}$$

the elastic moduli of the composite material is:

$$E_{\text{hom}} = fE_f + (1-f)E_m; \tag{39}$$

the density of the composite material is:

$$\rho_{\text{hom}} = f\rho_f + (1-f)\rho_m; \tag{40}$$

and moment of inertia is:

$$I = \frac{b\,h^3}{12}. \tag{41}$$

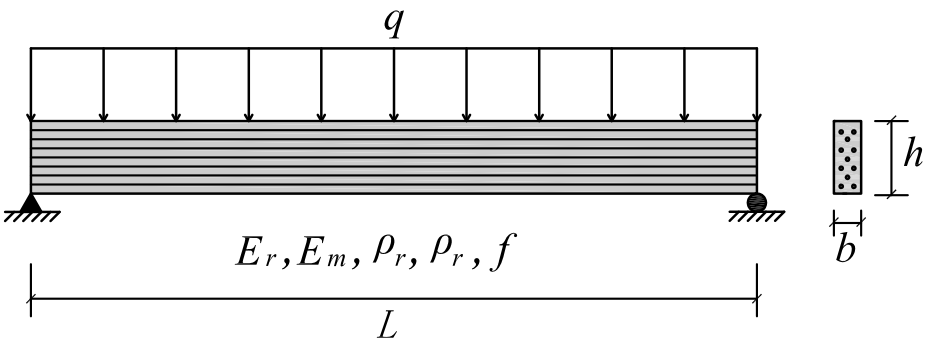

Fig. 2. Simply supported composite beam.

For this composite beam, a total of 8 uncertain parameters considered are summarized in Tab. II. The proposed GPM UQ method is launched to calculate the mean and variance of the maximal mid-span displacement d under those 8 uncertain parameters. To the end of verification of the GPM method, the brute-force MCS approach is utilized to approximate the true values of statistics of the displacement d. And a large number of samples, namely 10^6, are adopted in order to ensure that the mean and variance are convergent. The UQ task is carried out on desktop platform of LENOVO M4360-N000 with Pentium (R) D CPU G2030 @ 3.00 GHz, so do the following two examples.

DOI: 10.1002/nme

Tab. II. Characteristics of parameters of the composite beam [39].

No.	Parameter	Distribution	Mean	COV
1	Length (L)	Log-normal	2 (m)	0.01
2	Widht of the rectangular section (b)	Log-normal	10 (cm)	0.03
3	Height of the rectangular section (h)	Log-normal	1 (cm)	0.03
4	Elastic moduli of the fiber material (E_f)	Log-normal	3.0E+11 (Pa)	0.15
5	Elastic moduli of the matrix matrial (E_m)	Log-normal	1.0E+10 (Pa)	0.15
6	Density of the fiber material (ρ_f)	Log-normal	1800 (kg/m^3)	0.03
7	Density of the matrix matrial (ρ_m)	Log-normal	1200 (kg/m^3)	0.03
8	Fraction (f)	Beta	0.5	0.10

Note: COV, namely the coefficient of variation, represents the ratio of the standard deviation to the mean.

Tab. III. UQ results for the composite beam.

QoI	GPM method		MCS		Relative error (%)	
	Mean	Variance	Mean	Variance	Mean	Variance
d (mm)	2.4460	0.1944	2.4462	0.1950	0.0109	0.2797
Time (sec)	30.9		4.4		-	

Note: Relative error=$|(\text{GPM} - \text{MCS})/\text{MCS}|$

Tab. III summarizes the results of UQ for the composite beam. As seen in Tab. III, the results of GPM method have an excellent agreement with the results of MCS, and particularly, the relative errors of mean and variance are 0.0109% and 0.2797%, respectively, which indicates that the proposed GPM UQ method is effective and reliable. Beyond the accuracy of the proposed method, its computational efficiency also needs to be concerned with. The whole UQ task performed by the GPM method takes around half min, which means that the proposed GPM method is considerably computationally efficient. It should be pointed out that although the computational time of the brute-force MCS is 4.4 sec, it does not mean that the brute-force MCS is generally efficient. The short time of the brute-force MCS is in essence attributable to the fact that input-output relationship defined in Eq. (37) is extremely simple rather than black-box so that the performing brute-force MCS is quite straightforward, and direct model evaluations do not cost much time. When applied to the complex systems, the brute-force likely tends to be neither affordable nor feasible, which will be confirmed in the subsequent two cases.

Considering the fact that the number of Gaussian quadrature points have an impact on the integration result, which can be implied by Eq. (24), we explore how UQ results are influenced by the number of Gaussian quadrature points. Here we define an index of total absolute error as:

$$TAE = \sum_{i=1}^{k} \left(\left| E^i_{\text{GPM}} - E^i_{\text{MCS}} \right| + \left| V^i_{\text{GPM}} - V^i_{\text{MCS}} \right| \right) \tag{42}$$

where k represents the number of QoIs; E and V denote mean and variance, respectively.

The relationship between TAE and the number of Gaussian quadrature points as well as the associated computational time are shown in Fig. 3. In light of Fig. 3, we can have two observations: (1) the index TAE becomes stable after the number 10, which means that UQ results by the GPM method is convergent; and (2) the increase in the number from 5 to 100 do not result in the big increase of the computation cost. The second observation is due to the fact that Gaussian quadrature is remarkably computationally efficient especially with the use of fast Fejér Type-2 quadrature rules. Nevertheless, it may be too early to draw the conclusion that the increased number of Gaussian quadratures will not result in the obvious increase in the computational cost. We will further check this observation in the subsequent more complex engineering examples.

DOI: 10.1002/nme

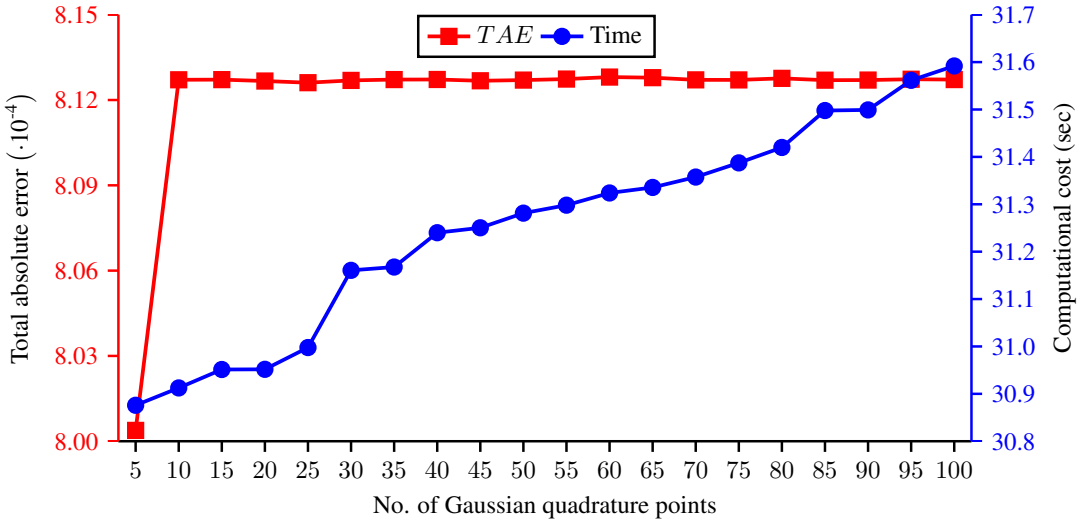

Fig. 3. Total absolute error and computational time of the composite beam versus the number of Gaussian quadrature points.

4.2. Case II: An auto frame

The second test-bed to validate the proposed GPM UQ method is an auto frame, which is composed of two main frames and six diaphragms. The geometric details of the auto frame are shown in Fig. 4. All the components of the auto frame have the identical thickness (T), whose nominal value is 5 mm. The nominal values of elastic moduli and density are corresponding to 2.1E+11 Pa and 7860 kg/m^3, respectively. The finite element model (FEM) of the auto frame is constructed using FEA package ANSYS [40]. All of the components are modeled as shell elements (SHELL63). The FEM consists of a total of 6707 nodes and 6180 elements, and the resulting total number of degrees of freedom (DOFs) is 40242. The first four natural frequencies are our focus. The FEM and the first four mode shapes are presented in Fig. 5.

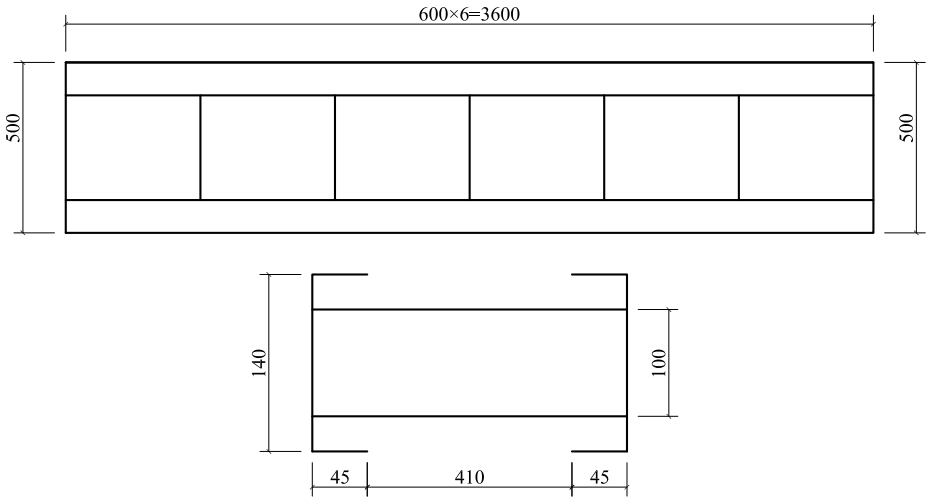

Fig. 4. Configuration of the auto frame: plan (top) and side (bottom) (unit: mm).

DOI: 10.1002/nme

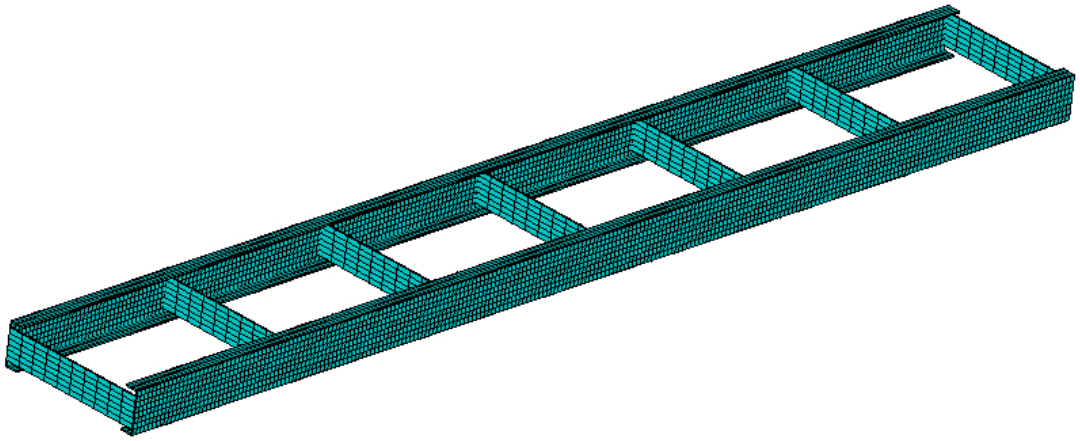

(a) FEM

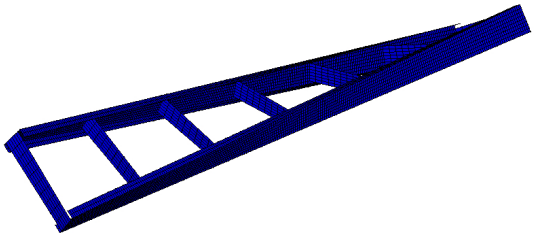

(b) First torsional mode ($f_1 = 6.156$ Hz)

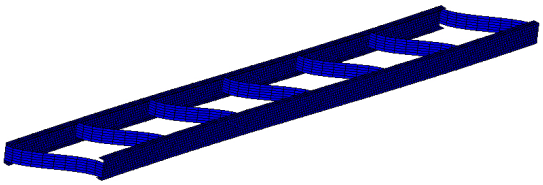

(c) First longitudinal mode ($f_2 = 14.338$ Hz)

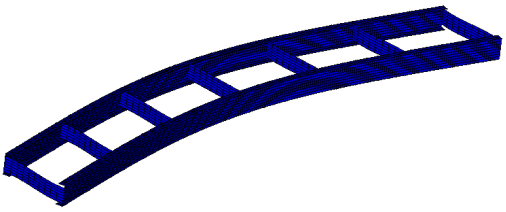

(d) First vertical mode ($f_3 = 16.825$ Hz)

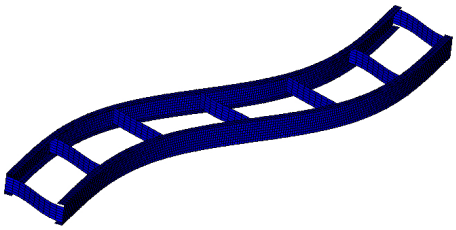

(e) Second vertical mode ($f_4 = 43.729$ Hz)

Fig. 5. FEM and mode shapes of the auto frame with mean value of uncertain parameters.

A total of 3 parameters including material properties: elastic moduli (E) and density (ρ), and geometric property: thickness (T) are assumed to be uncertain. Their statistical characteristics are listed in Tab. IV. Then the GPM method is put forward to evaluate the mean and variance of the first four natural frequencies of the auto frame subjected to parameter uncertainty. Meanwhile, like the previous example, the brute-force MCS with sample size 10^6 is still used as the metric for accuracy assessment of the GPM approach. The corresponding results are tabulated in Tab. V, from which we know that the largest relative errors in the mean and variance compared to the "true" values approximated by the brute-force MCS method are 0.0015% and 0.1309%, respectively. The nearly negligible relative errors demonstrate that the statistics of the four natural frequencies derived by our method are almost the same as those obtained by the brute-force MCS, which verifies that the proposed GPM method is effective and reliable for UQ. In terms of the computational time, the GPM presents overwhelming superiority over the brute-force MCS. To be specific, the former takes 904.0 sec while the latter is 2815186.5 sec (around 32.6 days). Therefore, it can be concluded that the GPM method is very accurate and computationally efficient as well, whereas the computational efficiency of the brute-force MCS is unacceptable.

DOI: 10.1002/nme

Tab. IV. Characteristics of parameters of the auto frame.

No.	Parameter	Distribution	Mean	COV
1	Elastic moduli (E)	Log-normal	2.1E+11 (Pa)	0.15
2	Density (ρ)	Weibull	7860 (kg/m^3)	0.10
3	Thickness (T)	Uniform	5 (mm)	0.10

Tab. V. UQ results for the auto frame.

QoI	GPM method		MCS		Relative error (%)	
	Mean	Variance	Mean	Variance	Mean	Variance
f_1 (Hz)	6.2354	0.7218	6.2355	0.7222	0.0007	0.0640
f_2 (Hz)	14.5191	3.8509	14.5193	3.8547	0.0015	0.0993
f_3 (Hz)	17.0524	2.5470	17.0525	2.5497	0.0003	0.1067
f_4 (Hz)	44.3057	16.8525	44.3062	16.8746	0.0012	0.1309
Time (sec)	904.0		2815186.5		-	

Following the UQ task, an investigation of the impact of the number of Gaussian quadrature points on the UQ results of the GPM method is considered. The graph of the TAE and the computational time against the number of Gaussian quadrature points is shown in Fig. 6. Similar observations are obtained. That is, when the number of Gaussian quadrature points arrives at 10, TAE becomes convergent, and the increase in the number of Gaussian quadrature points from 5 to 100 do not give rise to the noticeable upsurge of the computational cost either.

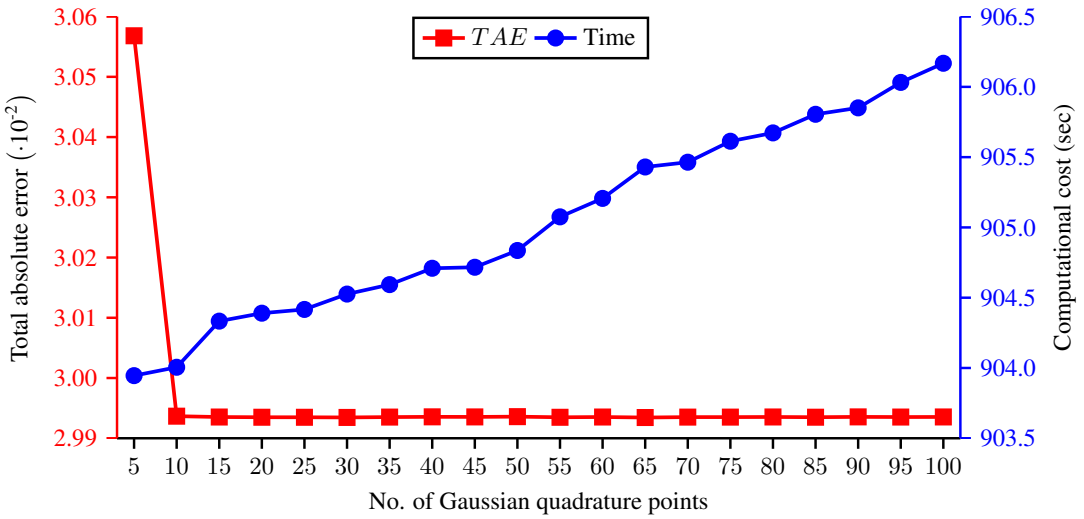

Fig. 6. Total absolute error and computational time of the auto frame versus the number of Gaussian quadrature points.

4.3. Case III: A CFST through arch bridge

A CFST through arch bridge is used as the third test-bed to verify the GPM UQ method. Fig. 7 shows the configuration of the CFST through arch bridge with a rise-to-span ratio of 1/6, which is 30 m in width and 65 m in length. The main girders are formed in a shape of a hollow box. The floor system, which comprises the 0.25 m thick concrete slab, is supported by T-shaped cross girders. The two parallel arch ribs lie in a vertical plane with the center-to-center distance of 21.5 m.

DOI: 10.1002/nme

The arch ribs have a constant wall thickness of 14 mm throughout their length, and are filled with concrete. Two symmetrical lateral bracings consisting of K-shaped hollow steel tube are placed to connect the vertical arch ribs, aiming at improving structural stability. The arch ribs and the floor system are vertically connected by 22 suspenders placed every 4.8 m, each having 73 steel wires with a diameter 7 mm. The arch bridge is modeled within the FEA package ANSYS environment. 3-D beam elements (BEAM188) are utilized to model the main girder, cross girder, and lateral bracing. The suspenders are modeled with elements (LINK10). Shell elements (SHELL63) are used to simulate the bridge deck. In sum, the constructed FEM has a total of 379 nodes and 724 elements, including 196 shell elements, 506 beam elements, and 22 link elements, and the resulting total number of DOFs is 2250. Herein, the first four natural frequencies are our QoIs. Fig. 8 shows the FEM and the first four mode shapes of the CFST through arch bridge.

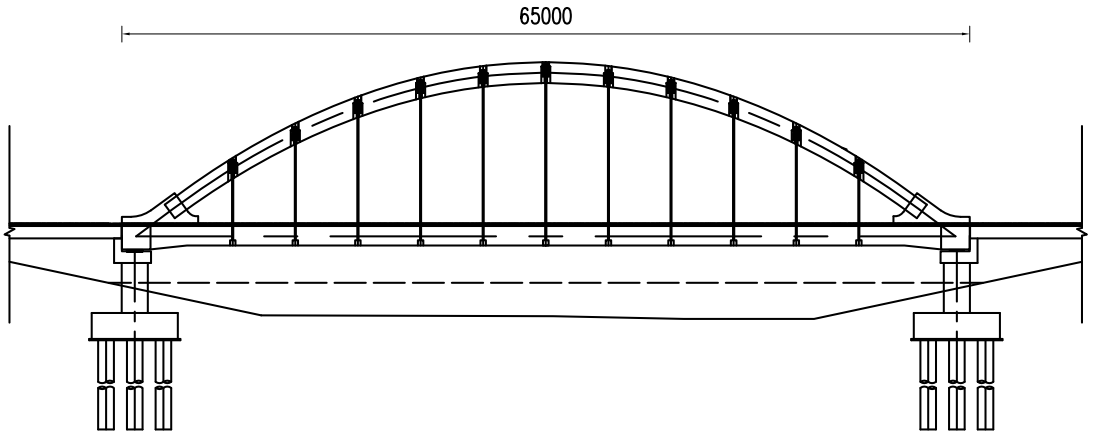

(a) Elevation

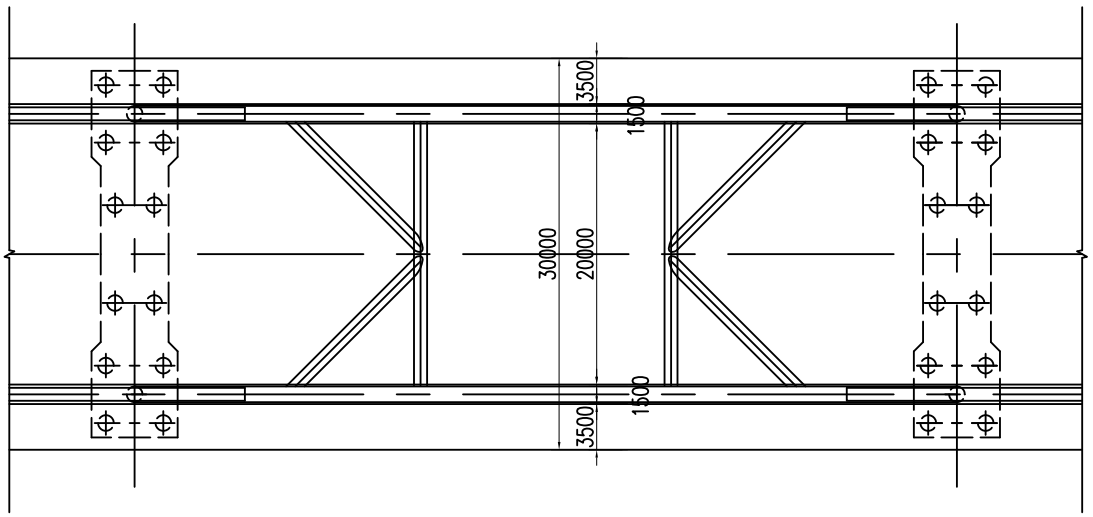

(b) Plan

Fig. 7. Configuration of the CFST arch bridge (unit: mm).

DOI: 10.1002/nme

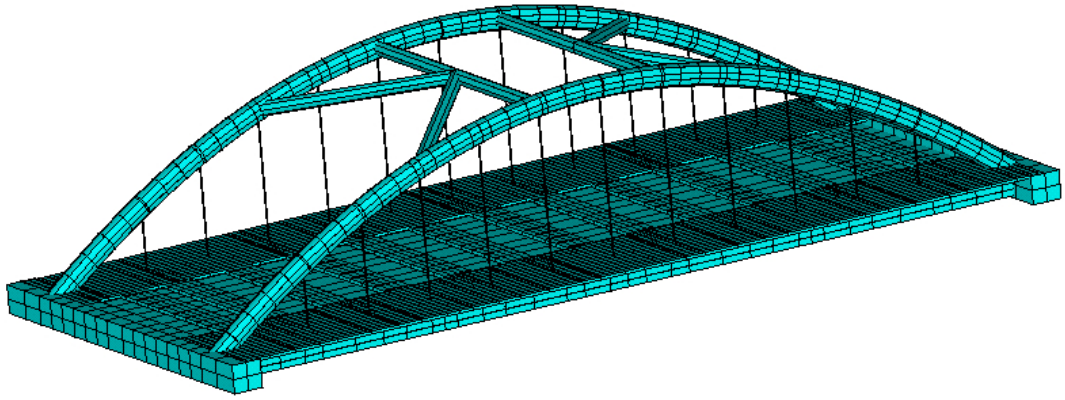

(a) FEM

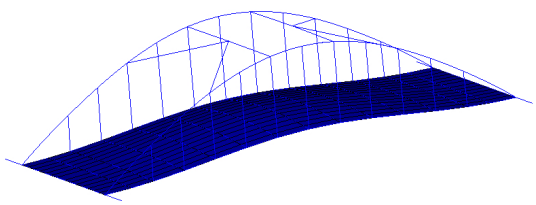

(b) First vertical mode ($f_1 = 2.764$ Hz)

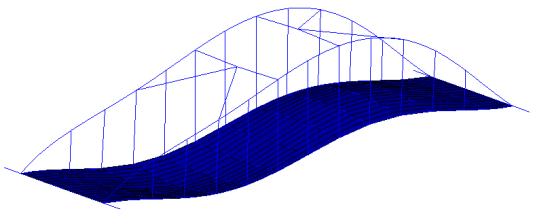

(c) Second vertical mode ($f_2 = 3.412$ Hz)

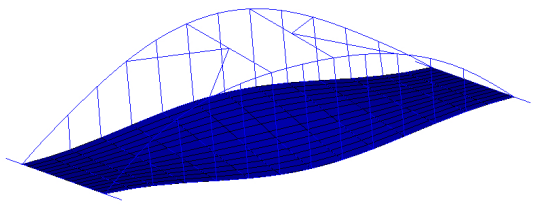

(d) First torsional mode ($f_3 = 3.887$ Hz)

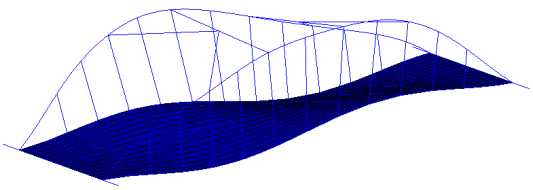

(e) Second torsional mode ($f_4 = 4.809$ Hz)

Fig. 8. FEM and mode shapes of the CFST through arch bridge with mean value of uncertain parameters.

Consider a total of 12 uncertain structural parameters, whose statistical characteristics are summarized in Tab. VI. These uncertain parameters comprise material and geometric properties related to the different structural components, such as main girder, deck, and arch rib. The GPM method is employed to quantify the uncertainty in the first four natural frequencies propagated from the parameter uncertainty. And in the meantime, the brute-force MCS with sample size 10^6 is performed for the purpose of accuracy assessment of the GPM method. The comparison of UQ results of the GPM method and the brute-force MCS is presented in Tab. VII. The extremely small differences between their UQ results indicate that the GPM method still has high accuracy for UQ of complex system. For the computational cost, the GPM method takes 431.7 sec while the brute-force MCS takes 224503.8 sec (around 2.6 days). Thus, one can conclude that the GPM method substantially alleviates the computational burden of UQ of complex system, while still achieving comparable accuracy to the brute-force MCS.

DOI: 10.1002/nme

Tab. VI. Characteristics of parameters of the CFST arch bridge.

No.	Parameter	Distribution	Mean	COV
1	Elastic moduli of stell used in arch rib (E_s)	Log-normal	2.1E+11 (Pa)	0.15
2	Elastic moduli of concrete inside arch rib (E_c)	Log-normal	3.5E+10 (Pa)	0.15
3	Density of concrete inside arch rib (ρ_c)	Weibull	2550 (kg/m^3)	0.10
4	Elastic moduli of cross girder (E_{cg})	Log-normal	3.5E+10 (Pa)	0.15
5	Density of cross girder (ρ_{cg})	Weibull	2500 (kg/m^3)	0.10
6	Elastic moduli of main girder (E_{mg})	Log-normal	3.5E+10 (Pa)	0.15
7	Density of main girder (ρ_{mg})	Weibull	2500 (kg/m^3)	0.10
8	Elastic moduli of lateral bracing (E_{lb})	Log-normal	2.1E+11 (Pa)	0.15
9	Elastic moduli of bridge deck (ρ_{bd})	Log-normal	2.8E+10 (Pa)	0.15
10	Thickness of bridge deck (T_{bd})	Uniform	0.25 (m)	0.10
11	Elastic moduli of suspender (E_{sp})	Log-normal	2.05E+11 (Pa)	0.15
12	Sectional area of suspender (A_{sp})	Normal	0.002809 (m^2)	0.05

Tab. VII. UQ results for the CFST arch bridge.

QoI	GPM method		MCS		Relative error (%)	
	Mean	Variance	Mean	Variance	Mean	Variance
f_1 (Hz)	2.7517	0.0187	2.7518	0.0188	0.0017	0.2127
f_2 (Hz)	3.4018	0.0437	3.4014	0.0432	0.0136	1.1663
f_3 (Hz)	3.7804	0.0308	3.7885	0.0302	0.2119	2.0319
f_4 (Hz)	4.7738	0.0557	4.7777	0.0547	0.0804	1.7936
Time (sec)	431.7		224503.8		-	

Subsequently, we turn to the study on the influence of the number of Gaussian quadrature points on the UQ results of the GPM method. The TAE and the corresponding computational time with respect to the number of Gaussian quadrature points is given in Fig. 9, from which we can see that TAE converge at the number of Gaussian quadrature points of 15, and the increase in the number of Gaussian quadrature points leads to the slight increase of the computational time.

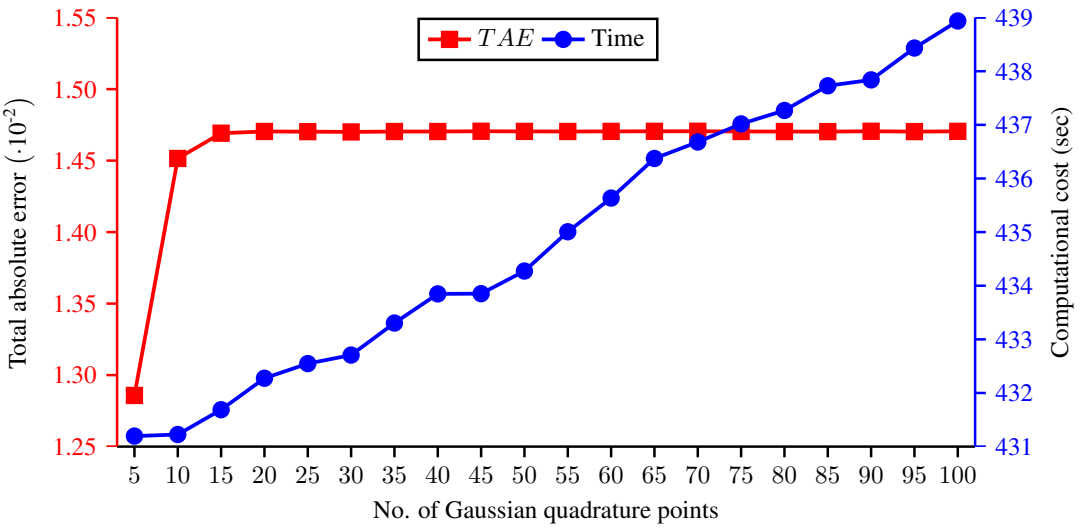

Fig. 9. Total absolute error and computational time of the CFST through arch bridge versus the number of Gaussian quadrature points.

DOI: 10.1002/nme

4.4. Discussion

This section provided three industrial examples of one composite beam, one auto frame, and one CFST through arch bridge to evaluate the capability of the proposed GPM method in UQ of complex systems. MCS, is used as the benchmark solution. The comparison of the GPM method and full MCS verifies that the GPM method presents an excellent performance in terms of both the computational accuracy and efficiency. The computational cost of these three examples is summarized in Tab. VIII, which reveals that as the simulation model of target structure becomes more complex, the computational cost of MCS exponentially grows. For example, MCS for UQ of the auto frame modeled by FEM with a total of 40242 DOFs takes about 32.6 days, which is highly undesirable in terms of computational efficiency. It is worth noting that the reason why the computational time of the MCS for the CFST through arch bridge is not as high as that of the auto frame is that the FEM of auto frame has a total of 40242 DOFs, which is about 18 times as many as the DOFs of FEM of the CFST through arch bridge. On the contrary, the present GPM method is quite computationally efficient and the increase of parameter dimensionality from 3 to 12 will not lead to the exponential growth of the computational time. In addition, it can be known from Tab. VIII that when applied to a complex system, a large share of the computational cost of UQ using GPM method is allocated to training set preparation by running the computationally expensive physical model. Therefore, we can conclude that the present GPM method itself for UQ is with great efficiency and provides a competitive alternative to solve the issue of the high computational cost involved in the UQ of complex systems.

For these examples, after UQ task, we investigate the impact of the number of Gaussian quadrature points on the accuracy of GPM method. Results show that the GPM method may become convergent at a low number of Gaussian quadrature points. In these examples, the convergence is reached at 10 or 15. Additionally, the big increase of the number of Gaussian quadrature points will not cause the exponential growth of the computational time. Accordingly, there may be no need to worry too much about the high computational cost resulting from the selected big number of Gaussian quadrature points for the sake of high accuracy of the GPM method.

Tab. VIII. Computational cost summary of three cases.

Case	No. of parameters	Computational cost (sec)	
		GPM method	MCS
Case I: A composite beam (a simple mathematical function)	8	30.9	4.4
Case II: An auto frame (a FEM with 40242 DOFs)	3	904	2815186.5
Case III: A CFST through arch bridge (a FEM with 2250 DOFs)	12	431.7	224503.8

5. CONCLUSIONS

A new GPM-based approach is developed for efficient calculation of mean and variance of QoIs of complex systems in this paper. This proposed GPM-based method is suitable for the cases whose uncertain parameters are arbitrarily distributed. The core of this methodology is that GPM is used as the surrogate model of the computationally expensive simulation model, which enables us to obtain the closed form expressions for the integrals related to mean and variance via decomposing high-dimensional integrals into one-dimensional integrals. Thus, for calculation of mean and variance of QoIs, we just have to compute the one-dimensional integrals rather than the daunting high-dimensional integrals, which is likely to be computationally intractable. These one-dimensional integrals can be evaluated in an analytical way when the parameters are either uniformly- or normally distributed. And when parameters do not follow or cannot be modeled with the above

DOI: 10.1002/nme

two specific probability distributions, the effective Gaussian quadrature technique is utilized for the fast computation of the one-dimensional integrals. As a consequence, the present GPM method is able to evaluate mean and variance of QoIs in a fast manner, thus allowing for efficient UQ of complex systems with arbitrary probability distributed parameters.

The proposed GPM method is applied to calculate mean and variance in three applications, where the output functions are either simple mathematical functions or eigenvalues of an auto frame and a CFST through arch bridge. MCS is used as benchmark solution to verify the feasibility of the proposed GPM method. The results demonstrate that the GPM is as accurate as MCS, but also offers considerable reduction in the computational cost. Therefore, the GPM method is effective and reliable for UQ of complex systems in terms of the computational accuracy and efficiency. In addition to UQ of three industrial examples, we also investigate on how the computational accuracy and time of GPM method are affected by the number of Gaussian quadrature points. The results of three examples confirm that a low number of Gaussian quadrature points are enough to ensure the GPM method convergent and the increase of the number will not cause the noticeable increase in the computational time. The latter observation implies that using large number of Gaussian quadrature points for the end of high accuracy will not lead to the high computational cost.

ACKNOWLEDGEMENT

This research was financially supported by the National Science Foundation of China (Grant No. 51508144), the Anhui Provincial Natural Science Foundation (Grant No. 1608085QE118), and the China Postdoctoral Science Foundation (Grant No. 2015M581981). Constructive comments from anonymous reviewers are also gratefully acknowledged.

REFERENCES

1. Wan HP, Mao Z, Todd MD, Ren WX. Analytical uncertainty quantification for modal frequencies with structural parameter uncertainty using a Gaussian process metamodel. *Engineering Structures* 2014;75:577-589.
2. Helton J, Davis F. Latin hypercube sampling and the propagation of uncertainty in analyses of complex systems. *Reliability Engineering & System Safety* 2003;81(1):23-69.
3. Saltelli A, Annoni P, Azzini I, Campolongo F, Ratto M, Tarantola S. Variance based sensitivity analysis of model output. design and estimator for the total sensitivity index. *Computer Physics Communications* 2010;181(2):259-270.
4. Székely GS, Schuëller GI. Computational procedure for a fast calculation of eigenvectors and eigenvalues of structures with random properties. *Computer Methods in Applied Mechanics and Engineering* 2001;191(8-10):799-816.
5. Au SK, Beck JL. Estimation of small failure probabilities in high dimensions by subset simulation. *Probabilistic Engineering Mechanics* 2001;16(4):263-277.
6. Xiu D, Karniadakis GE. The Wiener-Askey polynomial chaos for stochastic differential equations. *SIAM journal on scientific computing* 2002; 24(2):619-644.
7. Ghanem R G, Spanos P D. *Stochastic finite elements: a spectral approach*. Courier Corporation; 2003.
8. Babuska I, Tempone R, Zouraris GE. Galerkin finite element approximations of stochastic elliptic partial differential equations. *SIAM Journal on Numerical Analysis* 2004; 42(2):800-825.
9. Matthies HG, Keese A. Galerkin methods for linear and nonlinear elliptic stochastic partial differential equations. *Computer Methods in Applied Mechanics and Engineering* 2005; 194(12):1295-1331.
10. Najm HN. Uncertainty quantification and polynomial chaos techniques in computational fluid dynamics. *Annual Review of Fluid Mechanics* 2009; 41(1):35-52.
11. Ghosh D, Ghanem R. An invariant subspace-based approach to the random eigenvalue problem of systems with clustered spectrum. *International Journal for Numerical Methods in Engineering* 2012;91(4):378-396.
12. Oladyshkin S, Nowak W. Data-driven uncertainty quantification using the arbitrary polynomial chaos expansion. *Reliability Engineering & System Safety* 2012;106:179-190.
13. Lopez RH, Fadel Miguel LF, Souza de Cursi JE. Uncertainty quantification for algebraic systems of equations. *Computers & Structures* 2013;128:189-202.
14. Adhikari S, Khodaparast HH. A spectral approach for fuzzy uncertainty propagation in finite element analysis. *Fuzzy Sets and Systems* 2013;243:1-24.
15. Yadav V, Rahman S. Uncertainty quantification of high-dimensional complex systems by multiplicative polynomial dimensional decompositions. *International Journal for Numerical Methods in Engineering* 2013;94(3):221-247.
16. Wu J, Luo Z, Zhang N, Zhang Y. A new uncertain analysis method and its application in vehicle dynamics. *Mechanical Systems and Signal Processing* 2015;50-51:659-675.
17. Xiu D. *Numerical methods for stochastic computations: A spectral method approach*. Princeton University Press; 2010. ISBN 1400835348.

DOI: 10.1002/nme

18. Ma X, Zabaras N. An adaptive hierarchical sparse grid collocation algorithm for the solution of stochastic differential equations. *Journal of Computational Physics* 2009;228(8):3084-3113.
19. Yadav V, Rahman S. Adaptive-sparse polynomial dimensional decomposition methods for high-dimensional stochastic computing. *Computer Methods in Applied Mechanics and Engineering* 2014;274:56-83.
20. Karagiannis G, Lin G. Selection of polynomial chaos bases via Bayesian model uncertainty methods with applications to sparse approximation of PDEs with stochastic inputs. *Journal of Computational Physics* 2014;259:114-134.
21. Fricker TE, Oakley JE, Sims ND, Worden K. Probabilistic uncertainty analysis of an FRF of a structure using a Gaussian process emulator. *Mechanical Systems and Signal Processing* 2011;25(8):2962-2975.
22. Xia Z, Tang J. Characterization of dynamic response of structures with uncertainty by using Gaussian processes. *Journal of Vibration and Acoustics* 2013;135(5):051006-051006.
23. DiazDelaO FA, Adhikari S, Saavedra Flores EI, Friswell MI. Stochastic structural dynamic analysis using Bayesian emulators. *Computers & Structures* 2013;120:24-32.
24. Lockwood B, Mavriplis D. Gradient-based methods for uncertainty quantification in hypersonic flows. *Computers & Fluids* 2013;85:27-38.
25. Bilionis I, Zabaras N, Konomi BA, Lin G. Multi-output separable Gaussian process: Towards an efficient, fully Bayesian paradigm for uncertainty quantification. *Journal of Computational Physics* 2013;241:212-239.
26. DiazDelaO FA, Adhikari S. Gaussian process emulators for the stochastic finite element method. *International Journal for Numerical Methods in Engineering* 2011;87(6):521-540.
27. Kundu A, DiazDelaO FA, Adhikari S, Friswell MI. A hybrid spectral and metamodeling approach for the stochastic finite element analysis of structural dynamic systems. *Computer Methods in Applied Mechanics and Engineering* 2014;270(3):201-219.
28. Rasmussen CE, Williams CKI. *Gaussian processes for machine learning*. MIT Press; 2006.
29. Sacks J, Welch WJ, Mitchell TJ, Wynn HP. Design and analysis of computer experiments. *Statistical Science* 1989;4(4):409-423.
30. Neal RM. *Regression and classification using Gaussian process priors*, in: J.M. Bernardo, J.O. Berger, et al. (Eds.) Bayesian Statistics 6: proceedings of the sixth Valencia international meeting, Oxford University Press, New York, 1999, pp. 476-501.
31. NPetersen KB,Pedersen MS. *The matrix cookbook*. Technical University of Denmark; 2008.
32. Wan HP, Ren WX. A residual-based Gaussian process model framework for finite element model updating. *Computers & Structures* 2015;156:149-159.
33. Gautschi W. *Orthogonal polynomials: computation and approximation*. Oxford University Press; 2004.
34. Fernandes AD, Atchley WR. Gaussian quadrature formulae for arbitrary positive measures. *Evolutionary Bioinformatics* 2006;2:251-259.
35. Gander MJ, Karp AH. Stable computation of high order Gauss quadrature rules using discretization for measures in radiation transfer. *Journal of Quantitative Spectroscopy and Radiative Transfer* 2001;68(2):213-223.
36. Gragg W, Harrod W. The numerically stable reconstruction of Jacobi matrices from spectral data. *Numerische Mathematik* 1984;44(3):317-335.
37. Waldvogel J. Fast construction of the Fejér and Clenshaw-Curtis quadrature rules. *BIT Numerical Mathematics* 2006;46(1):195-202.
38. Gautschi W. On generating orthogonal polynomials. *SIAM Journal on Scientific and Statistical Computing* 1982;3(3):289-317.
39. Caniou Y. *Global sensitivity analysis for nested and multiscale modelling*. Ph.D. thesis; Universit Blaise Pascal-Clermont-Ferrand II; 2012.
40. ANSYS. Users Manual, Revision 8.0. Swanson Analysis System; Houston, USA; 2003.

DOI: 10.1002/nme